

A comparison of graphene, superconductors and metals as conductors for metamaterials and plasmonics

Philippe Tassin^{1*}, Thomas Koschny¹, Maria Kafesaki² and Costas M. Soukoulis^{1,2}

¹ Ames Laboratory—U.S. DOE and Department of Physics and Astronomy, Iowa State University, Ames, IA 50011, USA

² Institute of Electronic Structure and Lasers (IESL), FORTH, 71110 Heraklion, Crete, Greece

* e-mail: tasssin@ameslab.gov

Supplementary Methods

Introduction

The foundation of our classification of materials lies in equation (1) of the main text,

$$\Pi = \frac{P_{\text{diss}}}{P_{\text{inc}}} = 2\pi \left(\frac{a_k}{\lambda_0} \right) \frac{F \tilde{\omega}^4 \zeta}{\left[\tilde{\omega}^2 (1 + \xi) - 1 \right]^2 + (\tilde{\omega} \zeta + \tau \tilde{\omega}^5)^2}, \quad (\text{S1})$$

which provides the dissipated power fraction of the metamaterial element. In this section, we derive this expression. We consider metamaterials that consist of conducting elements of subwavelength dimensions. A typical example of such an element is depicted in Supplementary Figure 1 in the form of an SRR for illustrative purposes, but the analysis below does not depend on the exact shape.

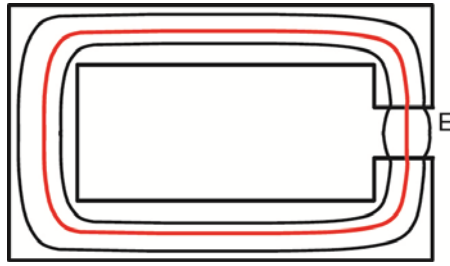
Derivation of the circuit equation

We start the derivation of the circuit equation from Faraday's law in integral form:

$$\oint \mathbf{E} \cdot d\mathbf{l} = -\frac{d}{dt} \iint \mathbf{B} \cdot d\mathbf{S}. \quad (\text{S2})$$

We choose the path of the contour integral along an electric field line in the conductor closed by an electric field line in the gap (see Supplementary Figure 1). The left-hand side of the above equation can be readily shown to equal the sum of the voltage across the resistor formed by the metallic element and the voltage across the capacitor formed by the gap:

$$\oint \mathbf{E} \cdot d\mathbf{l} = RI + \frac{1}{C} \int I dt. \quad (\text{S3})$$



Supplementary Figure 1 | A quasistatic metallic circuit. The curved lines are electric field lines along which the contour integral in equation (S2) must be integrated. The field lines follow the current density in the metal and the displacement field in the gap.

The right-hand side of equation (S2) contains a contribution from the incident field as well as a contribution from the magnetic field generated by the current in the circuit:

$$-\frac{d}{dt} \iint \mathbf{B} \cdot d\mathbf{S} = -\frac{d}{dt} \iint \mathbf{B}_{\text{inc}} \cdot d\mathbf{S} - \frac{d}{dt} \iint \mathbf{B}_{\text{circuit}} \cdot d\mathbf{S}. \quad (\text{S4})$$

Because the circuit is smaller than the wavelength, we can assume the incident magnetic field is constant over the circuit, such that the contribution from the incident field equals

$$-\frac{d}{dt} \iint \mathbf{B}_{\text{inc}} \cdot d\mathbf{S} = -\frac{d}{dt} (\mu_0 H_0 A \cos(\omega t)), \quad (\text{S5})$$

where A is the area enclosed by the circuit and H_0 is the magnetic field amplitude of the incident wave.

What remains is the contribution from the magnetic induction field generated by the current in the circuit. Again in the quasistatic approximation and after a second differentiation with respect to time, this leads to the circuit equation with the self-inductance term:

$$L \frac{d^2 I}{dt^2} + R \frac{dI}{dt} + \frac{1}{C} I = -\frac{d\mathcal{E}}{dt} = -\frac{d^2}{dt^2} (\mu_0 H_0 A \cos(\omega t)). \quad (\text{S6})$$

This is Kirchoff's equation describing the electrical current, I , flowing in the metallic circuit of each meta-atom, driven by the external time-dependent magnetic field of an incident electromagnetic wave. A is the area enclosed by the circuit, H_0 the magnetic field amplitude of the incident wave, and ω the frequency of the incident wave. The inductance, L , and capacitance, C , must be interpreted as effective values that encompass coupling between neighbouring circuits²⁴. The right-hand term in equation (S6) is of course nothing else than the electromotive force, \mathcal{E} , induced in the circuit by the incident field. Solving this equation yields a Lorentzian response function with a resonance at frequency $\omega_0 = 1/\sqrt{LC}$ and damping factor $\gamma = R/L$. If we now make the circuit from a conductive material with increasingly high conductivity, the resistance, R , becomes smaller and the damping factor goes to zero. The consequence is that the dissipated power at the resonance frequency becomes arbitrarily large, even larger than the power in the incident plane wave, which is clearly unphysical.

The reason behind this “dissipated power catastrophe” is that equation (S6) neglects that the circuit radiates energy away. The radiated power imposes a finite broadening of the resonance—even if the conducting material becomes (almost) lossless. To include radiation effects, we have to take a second look at the contribution of the circuit current to the electromotive force.

To that purpose, we start from the vector potential, \mathbf{A} , which takes the following form in the Lorentz gauge^{S1}:

$$\mathbf{A}(\mathbf{r}, t) = \frac{\mu_0}{4\pi} \iiint d^3\mathbf{r}' \int dt' \frac{\mathbf{J}(\mathbf{r}', t - |\mathbf{r} - \mathbf{r}'|/c)}{|\mathbf{r} - \mathbf{r}'|}. \quad (\text{S7})$$

Converting to the frequency domain, the vector potential takes the form

$$\mathbf{A}(\mathbf{r}) = \frac{\mu_0}{4\pi} \iiint \mathbf{J}(\mathbf{r}') \frac{e^{ik_0|\mathbf{r}-\mathbf{r}'|}}{|\mathbf{r}-\mathbf{r}'|} d^3\mathbf{r}', \quad (\text{S8})$$

where $k_0 = \omega/c$ is the free-space wave number and c is the speed of light in vacuum. The integral is over all currents, i.e., over the conducting medium. The magnetic induction field generated by the circuit currents can be obtained from $\mathbf{B} = \nabla \times \mathbf{A}$:

$$\mathbf{B}(\mathbf{r}) = -\frac{\mu_0}{4\pi} \iiint \mathbf{J}(\mathbf{r}') \times \frac{\mathbf{r} - \mathbf{r}'}{|\mathbf{r} - \mathbf{r}'|} \left(\frac{1}{|\mathbf{r} - \mathbf{r}'|} - ik_0 \right) \frac{e^{ik_0|\mathbf{r}-\mathbf{r}'|}}{|\mathbf{r} - \mathbf{r}'|} d^3\mathbf{r}'. \quad (\text{S9})$$

Since the conducting element is of subwavelength dimensions, all currents in the circuit are confined in a region sufficiently smaller than a wavelength, i.e. $|\mathbf{r} - \mathbf{r}'| \ll 2\pi/k_0$. This allows approximating the exponential function in equation (S9) by the first terms of its Taylor expansion in ik_0 . The lowest-order term yields

$$\mathbf{B}^{(0)}(\mathbf{r}) = -\frac{\mu_0}{4\pi} \iiint \mathbf{J}(\mathbf{r}') \times \frac{\mathbf{r} - \mathbf{r}'}{|\mathbf{r} - \mathbf{r}'|^3} d^3\mathbf{r}'. \quad (\text{S10})$$

This is Biot-Savart’s expression for the quasistatic field solution. It gives rise to the self-inductance term in the circuit equation and Neumann’s formula for the self-inductance^{S2}. The higher-order terms in $(ik_0)^m$ are

$$\mathbf{B}^{(m)}(\mathbf{r}) = -(ik_0)^m \frac{m-1}{m!} \frac{\mu_0}{4\pi} \iiint d^3\mathbf{r}' \mathbf{J}(\mathbf{r}') \times \frac{\mathbf{r} - \mathbf{r}'}{|\mathbf{r} - \mathbf{r}'|} |\mathbf{r} - \mathbf{r}'|^{m-2}. \quad (\text{S11})$$

The first-order term ($m = 1$) vanishes. The second-order term ($m = 2$) is an imaginary number and, thus, results in a reactive contribution to the impedance of the circuit. It will merely alter the resonance frequency of the circuit slightly. The third-order term is real and results in a resistive contribution to the impedance of the circuit. This is the term we need. In a sufficiently lossy circuit, this term can be neglected with respect to the voltage across the conductor. However, if we let the resistivity of the conducting medium become sufficiently small, the $m = 3$ term must be taken into consideration, since it becomes the leading term in the resistive part of the circuit impedance.

The third-order term yields

$$\begin{aligned} \mathbf{B}^{(3)}(\mathbf{r}) &= -(ik_0)^3 \frac{\mu_0}{12\pi} \iiint \mathbf{J}(\mathbf{r}') \times (\mathbf{r} - \mathbf{r}') d^3\mathbf{r}' \\ &= ik_0^3 \frac{\mu_0}{6\pi} \mathbf{m}, \end{aligned} \quad (\text{S12})$$

with \mathbf{m} the magnetic dipole moment of the circuit, and the electromotive force generated by this field becomes

$$-\frac{d}{dt} \iint \mathbf{B}^{(3)} \cdot d\mathbf{S} = i\omega \iint ik_0^3 \frac{\mu_0}{6\pi} \mathbf{m} \cdot d\mathbf{S} = -\frac{\mu_0 \omega^4 A^2}{6\pi c^3} I, \quad (\text{S13})$$

where A is the area enclosed by the circuit. With this additional term, we arrive at the circuit equation that includes the effects of the radiation reaction on the circuit:

$$L \frac{d^2 I}{dt^2} + (R + R_{\text{rad}}) \frac{dI}{dt} + \frac{1}{C} I = -\frac{d\mathcal{E}}{dt} = -\frac{d^2}{dt^2} (\mu_0 H_0 A \cos(\omega t)), \quad (\text{S14})$$

where the radiation resistance is given by

$$R_{\text{rad}} = \frac{\mu_0 \omega^4 A^2}{6\pi c^3}. \quad (\text{S15})$$

One can verify that this expression for the radiation resistance is the same as the radiation resistance of a subwavelength antenna as determined from the radiated power in the far-field zone^{S1}.

We have omitted here the magnetic fields from neighbouring circuits in the metamaterial. These neighbouring circuits will have mainly two consequences: there will be mutual coupling between the magnetic fields and there may be local field effects. Both effects have been studied by Gorkunov *et al.*²⁴, who show they lead to (i) a renormalization of the circuit parameters and (ii) the emergence of a Clausius-Mosotti functional form of the permeability. The result is that the resonance slightly differs from the Lorentzian shape and that the resonance frequency shifts somewhat. We can neglect these effects here in our comparison of conducting materials, because they are material-independent and will not affect the relative difference between materials.

Derivation of the magnetic susceptibility and the dissipated power

The circuit equation can be most easily solved in the frequency domain:

$$\left(-i\omega L + (R + R_{\text{rad}}) - \frac{1}{i\omega C} \right) I = i\omega A \mu_0 H_0. \quad (\text{S16})$$

Solving this equation for the induced current in the circuit yields

$$\begin{aligned}
 I &= -\frac{\omega^2 A \mu_0 H_0 / L}{\omega^2 + i\omega \left(\frac{R + R_{\text{rad}}}{L} \right) - \frac{1}{LC}} \\
 &= -\frac{\omega^2 A \mu_0 H_0 / L}{\omega^2 + i\omega \left(\frac{R + R_{\text{rad}}}{L} \right) - \omega_0^2}.
 \end{aligned}
 \tag{S17}$$

Each circuit has a magnetic dipole moment $m = A \times I$, and a metamaterial with N circuits per unit volume ($N = 1/V_{\text{uc}}$, where V_{uc} is the volume of a unit cell) has therefore a susceptibility of

$$\chi = -\frac{\omega^2 \mu_0 A^2 N / L}{\omega^2 + i\omega \left(\frac{R + R_{\text{rad}}}{L} \right) - \omega_0^2}.
 \tag{S18}$$

Introducing the filling factor

$$F = \mu_0 A^2 N / L,
 \tag{S19}$$

the susceptibility can be cast in the more customary form

$$\chi = -\frac{F \omega^2}{\omega^2 + i\omega \left(\frac{R + R_{\text{rad}}}{L} \right) - \omega_0^2}.
 \tag{S20}$$

The power dissipated by a single circuit can be found from the Ohmic heat formula:

$$\begin{aligned}
 P_{\text{diss}} &= \frac{1}{2} \text{Re}(R) |I|^2 \\
 &= \frac{1}{2} \frac{\omega^4 A^2 \mu_0^2 H_0^2 \text{Re}(R) / L^2}{\left(\omega^2 - \omega_0^2 \right)^2 + \omega^2 \left(\frac{R + R_{\text{rad}}}{L} \right)^2}.
 \end{aligned}
 \tag{S21}$$

Note, the dissipated power function broadens by the radiation resistance, but the radiated power itself is not a dissipation loss—it is, in fact, a much desired effect, since the radiated waves of all the circuits eventually combine to form the electromagnetic waves of the negative-permeability metamaterial. The optical power of the incident wave per unit cell equals

$$\begin{aligned}
 P_{\text{inc}} &= \frac{1}{2} E_0 H_0 a_E a_H \\
 &= \frac{1}{2} \mu_0 H_0^2 \frac{c}{N a_k},
 \end{aligned}
 \tag{S22}$$

where a_E , a_H , and a_k are the lattice constants along the electric field, the magnetic field, and the wave vector of the incident wave, respectively.

Combining equations (S21) and (S22), we eventually find the ratio of the dissipated power to the incident power:

$$\Pi = \frac{P_{\text{diss}}}{P_{\text{inc}}} = \frac{a_k}{c} \frac{\text{Re}(R)}{L} \frac{F\omega^4}{(\omega^2 - \omega_0^2)^2 + \omega^2 \left(\frac{R + R_{\text{rad}}}{L} \right)^2}. \quad (\text{S23})$$

Introduce dimensionless frequency

Finally, we introduce dimensionless variables to make the expressions independent of the frequency band of interest. This is achieved by normalizing the frequency to the geometric resonance frequency:

$$\tilde{\omega} = \frac{\omega}{\omega_0}. \quad (\text{S24})$$

In this way, the susceptibility can be written as

$$\chi = - \frac{F\tilde{\omega}^2}{\tilde{\omega}^2 - 1 + i\tilde{\omega} \left(\frac{R + R_{\text{rad}}}{\sqrt{L/C}} \right)}, \quad (\text{S25})$$

and the dissipated power fraction as

$$\Pi = \frac{P_{\text{diss}}}{P_{\text{inc}}} = 2\pi \left(\frac{a_k}{\lambda_0} \right) \frac{\text{Re}(R)}{\sqrt{L/C}} \frac{F\tilde{\omega}^4}{(\tilde{\omega}^2 - 1)^2 + \tilde{\omega}^2 \left(\frac{R + R_{\text{rad}}}{\sqrt{L/C}} \right)^2}. \quad (\text{S26})$$

Introduce the dimensionless variables ζ , ξ , and β

At finite frequencies, the resistivity and, hence, the resistance, R , are complex quantities, due to the finite mass of the charge carriers. Therefore, we define two variables, for the real and the imaginary part of the resistance, respectively:

- Dissipation factor:

$$\zeta = \frac{\text{Re}(R)}{\sqrt{L/C}} \quad (\text{S27})$$

- Kinetic inductance factor:

$$\xi = - \frac{\text{Im}(R)}{\tilde{\omega}\sqrt{L/C}} \quad (\text{S28})$$

- Radiation loss parameter:

$$\tau\tilde{\omega}^4 = \frac{R_{\text{rad}}}{\sqrt{L/C}} = \frac{\mu_0\omega^4 A^2}{6\pi c^3 \sqrt{L/C}} = \frac{1}{6\pi} \frac{\sqrt{\mu_0/\epsilon_0}}{\sqrt{L/C}} \frac{\omega_0^4 A^2}{c^4} \tilde{\omega}^4 \quad (\text{S29})$$

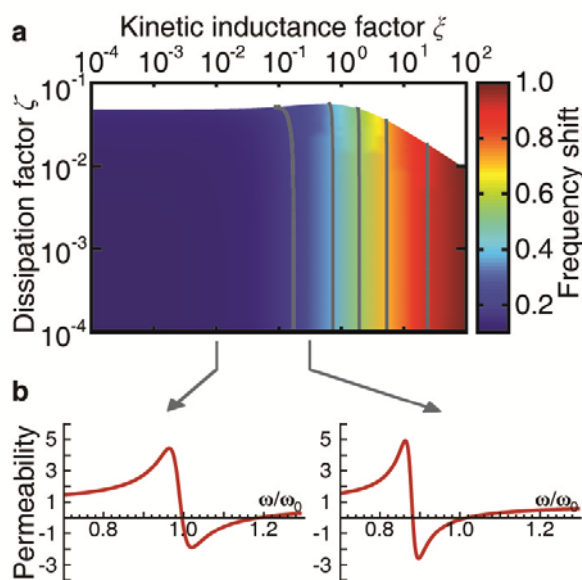
In terms of these dimensionless parameters, the susceptibility and dissipated power loss fraction are

$$\chi = -\frac{F\tilde{\omega}^2}{\tilde{\omega}^2(1+\xi)-1+i(\tilde{\omega}\zeta+\tau\tilde{\omega}^5)} \quad (\text{S30})$$

and

$$\Pi = \frac{P_{\text{diss}}}{P_{\text{inc}}} = 2\pi \left(\frac{a_k}{\lambda_0} \right) \frac{F\tilde{\omega}^4\zeta}{[\tilde{\omega}^2(1+\xi)-1]^2 + (\tilde{\omega}\zeta + \tau\tilde{\omega}^5)^2} \rightarrow \text{equation (1)} \quad (\text{S31})$$

The dissipation factor ζ is a dimensionless quantity determining the dissipative loss. This is discussed in the main text (figure 1) and forms the basis for our classification of conducting materials for use in resonant metamaterials.

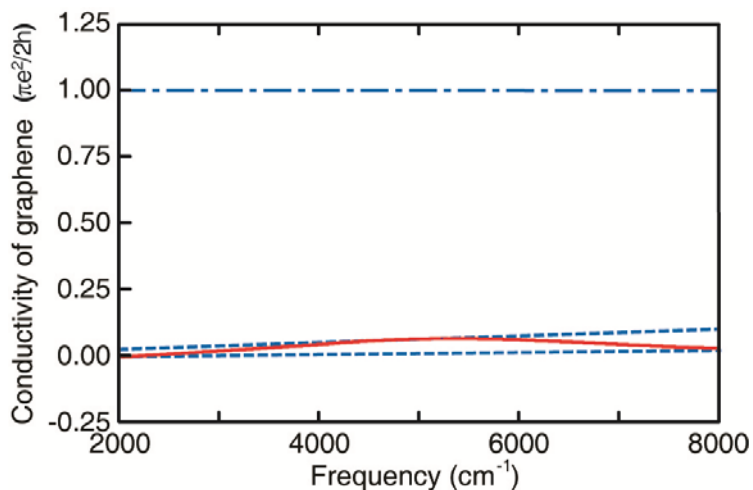


Supplementary Figure 2 | Frequency redshift in a metamaterial with $F = 0.37$ and $\tau = 0.039$; quantities are calculated for the slab-wire pair of figure 2a. **a**, Contour plot indicating how much the frequency at which $\mu(\omega) = -1$ is redshifted due to the kinetic inductance effect and the dissipation factor. The contour lines are approximately vertical, signifying that the resonance frequency depends only on the kinetic inductance factor to good approximation. The white region is the cut-off region where the resonance is too shallow to obtain negative permeability $\mu(\omega) = -1$. **b**, Resonance shapes of the magnetic permeability for kinetic inductance factors $\xi = 0.01$ and $\xi = 0.3$. The dissipation factor was taken as $\zeta = 0.02$. The strength of the resonance is almost unaltered by the kinetic inductance.

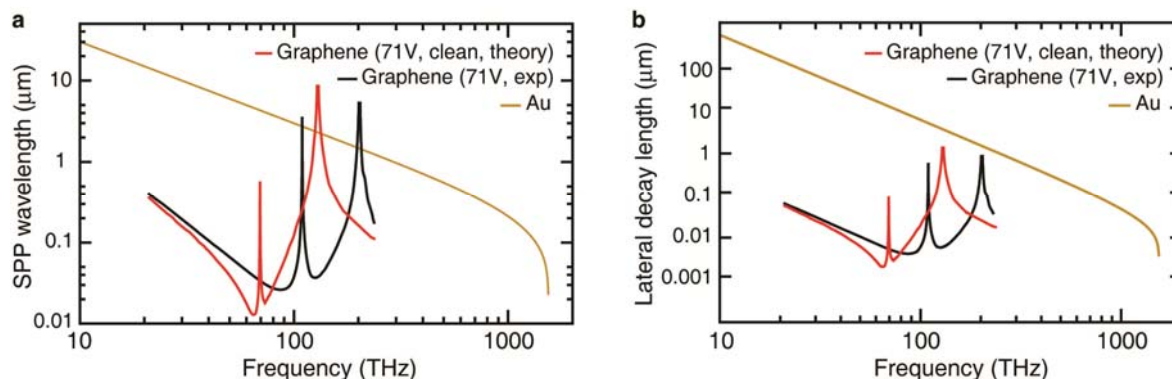
The kinetic inductance factor determines the saturation of the resonance frequency of negative-permeability metamaterials when they are scaled down towards optical frequencies^{33,31}. This effect is due to the contribution of the kinetic inductance of the free electrons or, in other words, to the mass inertia of the charge carriers. This is a material

effect and should be reflected in our model. To this end, we plot in Supplementary Figure 2a the frequency at which the desired magnetic permeability ($\mu = -1$) is realized as a function of the parameters ζ and ξ . First, the plot reveals that the frequency is essentially independent of the dissipation factor ζ . When the kinetic inductance factor is small, the resonance occurs at approximately $\omega = \omega_0$ and the frequency at which $\mu = -1$ is slightly larger. If the kinetic inductance factor is increased to a value of the order of unity, the resonance frequency is moved to smaller values (and the width of the negative permeability band decreases). This effect is confirmed by the permeability graphs in Supplementary Figure 2b.

Supplementary Figures and Table



Supplementary Figure 3 | Surface conductivity of charge-neutral graphene from reference 36. Blue, dash-dotted line: real part of the surface conductivity (measured and fitted curves coincide). Red line: measured imaginary part of the surface conductivity. Blue, dashed lines: fitted curves representing an upper and lower bound to the measured data for the imaginary part of the surface conductivity.



Supplementary Figure 4 | Surface plasmon polaritons on graphene and gold. The results for gold are for a 30 nm thick film at room temperature. The results for graphene are for strongly biased graphene calculated from experimental conductivity data (from ref. 36) and calculated from theoretical conductivity data that incorporates electron-electron interactions (from ref. 42). **a**, The wavelength of a surface plasmon polariton on graphene. Around 30 THz, the wavelength of SPPs on graphene is much smaller than the free-space wavelength $\lambda_0 = 2\pi c/\omega$. This is an immediate consequence of the large kinetic inductance of graphene as quantified by the kinetic inductance factor shown in figure 2c. **b**, Lateral confinement (away from the surface) of surface plasmon polaritons. The high kinetic inductance of graphene results in very good confinement with sub-micrometer decay length at mid-infrared frequencies.

Supplementary Table 1 | Plasma frequency, collision frequency, and resistivity of the metals and conducting oxides shown in figure 5. The numbers between parentheses refer to the literature where the data were obtained from; the quantities without references have been derived by us. We note again that the collision frequency includes all possible scattering mechanisms and is therefore frequency-dependent. The following labels are used to indicate the frequency/wavelength at which the data are evaluated: GHz (1 GHz), IR (1.55 μm), and VIS (500 nm).

	ω_p (Trad/s)	Γ (THz)	Re(ρ) (Ωm)
Ag (GHz)	13634 (S3)	26.6	1.62E-08 (S4)
Ag (IR)	13634 (S3)	28.8	1.75E-08 (S5)
Ag (VIS)	13634 (S3)	131	7.99E-08 (S5)
Al (GHz)	24001 (S3)	138	2.71E-08 (S6)
Al (IR)	24001 (S3)	321	6.30E-08 (S5)
Al (VIS)	24001 (S3)	930	1.82E-07 (S5)
Au (GHz)	13697 (S3)	37.5	2.26E-08 (S4)
Au (IR, Ordal)	13697 (S3)	81.4	4.90E-08 (S6)
Au (IR, J&C)	13697 (S3)	125	7.54E-08 (S5)
Au(VIS)	13697 (S3)	7095	4.27E-06 (S5)
AZO (GHz)	1602 (S7)	11364	5.00E-04 (S8)
Be (GHz)	28023 (S3)	257	3.70E-08 (S4)
Cr (GHz)	6911 (S9)	13.2 (S9)	3.12E-08
Cr (IR)	6911 (S9)	1087	2.57E-06 (S10)
Cr (VIS)	6911 (S9)	403	9.53E-07 (S11)
Cu (GHz)	16399 (S3)	40.8	1.71E-08 (S4)
Cu (IR)	16399 (S3)	253	1.06E-07 (S5)
Cu (VIS)	16399 (S3)	5803	2.44E-06 (S5)
ITO (GHz+IR)	1602 (S12)	145 (S12)	6.37E-06
K (GHz)	5648 (S3)	20.9	7.39E-08 (S4)
K(IR)	5648 (S3)	29.1	1.03E-07 (S11)
K(VIS)	5648 (S3)	145	5.15E-07 (S11)
KAu (GHz)	2339 (S13)	34.0	7.01E-07 (S13)
KAu (IR)	2339 (S13)	36.0	7.42E-07 (S13)
KAu (VIS)	2339 (S13)	84.8	1.75E-06 (S13)

Supplementary Table 1 | Continued.

	ω_p (Trad/s)	Γ (THz)	Re(ρ) (Ωm)
Li (GHz)	9738 (S14)	79.5	9.47E-08 (S4)
Li (IR)	9738 (S14)	209	2.49E-07 (S11)
Li (VIS)	9738 (S14)	691	8.23E-07 (S11)
LiAg (GHz)	11060 (S13)	82.1	7.58E-08 (S13)
LiAg (IR)	11060 (S13)	438	4.04E-07 (S13)
LiAg (VIS)	11060 (S13)	764	7.05E-07 (S13)
Na (GHz)	8168 (S15)	28.8	4.88E-08 (S4)
Na (IR)	8168 (S15)	50.1	8.48E-08 (S13)
Na (VIS)	8168 (S15)	174	2.94E-07 (S13)
Pd (GHz)	8293 (S6)	65.4	1.07E-07 (S4)
Pt	7791 (S6)	56.0 (S6)	1.04E-07
ZrN (IR)	11812 (S16)	70.3 (S16)	5.69E-08

References

- S1. Jackson, J. D. *Classical Electromagnetism* (Wiley, New York, 1962).
- S2. Reitz, J. R. & Milford, F. J. *Foundations of Electromagnetic Theory, 2nd Edition* (Addison-Wesley, Reading, 1967).
- S3. Fox, M. *Optical Properties of Solids* (Oxford Univ. Press, Oxford, 2001).
- S4. Haynes, W. M. *CRC Handbook of Chemistry and Physics, 92nd Edition* (CRC Press, Boca Raton, 2011).
- S5. Johnson, P. B. & Christy, R. W. Optical constants of the noble metals. *Phys. Rev. B* **6**, 4370-4379 (1972).
- S6. Ordal, M. A. & Bell, R. J., Alexander, R. W., Long, L. L. & Querry, M. R. Optical properties of fourteen metals in the infrared and far infrared: Al, Co, Cu, Au, Fe, Pb, Mo, Ni, Pd, Pt, Ag, Ti, V, and W. *Appl. Opt.* **24**, 4493-4499 (1985).
- S7. Rhodes, C. L. *et al.* Characterization of Monolayer Formation on Aluminum-Doped Zinc Oxide Thin Films. *Langmuir* **24**, 433-440 (2008).
- S8. Galca, A. C., Secu, M., Vlad, A. & Pedarnig, J. D. Optical properties of zinc oxide thin films doped with aluminum and lithium. *Thin Solid Films* **518**, 4603-4606 (2010).
- S9. Lovrincic, R. & Pucci, A. Infrared optical properties of chromium nanoscale films with a phase transition. *Phys. Rev. B* **80**, 205404 (2009).
- S10. Bos, L. W. & Lynch, D. W. Optical properties of antiferromagnetic chromium and dilute Cr-Mn and Cr-Re alloys. *Phys. Rev. B* **2**, 4567-4577 (1970).
- S11. Lynch, D. W. & Hunter, W. R. in *Handbook of Optical Constants of Solids II*, E. D. Palik, ed. (Academic Press, San Diego, 1991).
- S12. Chen, C.-W. *et al.* Frequency-dependent complex conductivities and dielectric responses of indium tin oxide thin films from the visible to the far-infrared. *IEEE J. Quant. Electron.* **46**, 1746-1754 (2010).
- S13. Blaber, M. G., Arnold, M. D. & Ford, M. J. Designing materials for plasmonic systems: the alkali-noble intermetallics. *J. Phys.: Condens. Matter* **22**, 095501 (2010).
- S14. Dugdale, J. S., Guban, D. & Okumura, K. The electrical resistivity of lithium-6. *Proc. R. Soc. Lond. A* **263**, 407-419 (1961).
- S15. Kittel, C. *Introduction to Solid State Physics* (Wiley, New York, ed. 17, 1996).
- S16. Veszelei, M., Andersson, K., Ribbing, C.-G., Jarrendahl, K. & Arwin, H. Optical constants and Drude analysis of sputtered zirconium nitride films. *Appl. Opt.* **33**, 1993-2001 (1994).